Vertical Transmission of Bovine H5N1 during Pregnancy and Lactation in Mice

Brittany A. Seibert[1†], Maclaine A. Parish[1†], Sattya N. Talukdar[1], Tianle Zhang[1], Sabal Chaulagain[1], Jennifer A. Liu[1], Jaiprasath Sachithanandham[1], Cosette Schneider[2], Lynda Coughlan[2,3], Andrew S. Bowman[4], Richard J. Webby[5], Jack R. Harkema[6], Andrew Pekosz[1], Sabra L. Klein[1,7,*]

Affiliations:

[1]W. Harry Feinstone Department of Molecular Microbiology and Immunology, Johns Hopkins Bloomberg School of Public Health, Baltimore, MD 21205, USA

[2]Department of Microbiology and Immunology, University of Maryland School of Medicine, Baltimore, MD 21205, USA

[3]Centre for Vaccine Development and Global Health (CVD), University of Maryland School of Medicine, Baltimore, MD 21201, USA

[4]Department of Veterinary Preventive Medicine, The College of Veterinary Medicine, The Ohio State University, Columbus, OH 43210, USA

[5]Department of Host-Microbe Interactions, St. Jude Children's Research Hospital, Memphis, TN 38105, USA

[6]Department of Pathobiology and Diagnostic Investigation, Michigan State University, East Lansing, MI 48824, USA

[7]Lead contact

*Correspondence: sklein2@jhu.edu (SLK)

†Authors contributed equally to this work; Author order reflects relative contribution.

Summary:

Panzootic spillover of H5N1 virus clade 2.3.4.4b has resulted in expanded host range among placental mammals, with lactation transmission via milk documented. Whether infection during pregnancy leads to *in utero* or lactational vertical transmission remains unknown. Pregnant outbred mice were infected with A/bovine/Ohio/B24OSU-472/2024 during the second or third trimester equivalent. Second trimester infection caused *in utero* infection, with infectious virus detected in the uterus, placenta, and fetus. Birth following third trimester infection resulted in offspring with decreased size and neurodevelopmental delays, with infectious virus detected in the neonatal milk ring and lungs as well as mammary tissues. Ongoing H5N1 infections present increased risk for human exposure and an H5N1 vertical transmission model in placental mammals is essential for understanding viral spread and evaluating treatments during pregnancy.

Introduction:

The evolving ecology of highly pathogenic avian influenza (HPAI) H5N1 involves increased mammalian infections. The outbreak of HPAI H5N1 clade 2.3.4.4b in U.S. dairy cattle, likely resulted from a single introduction of the B3.13 genotype virus from birds, followed by sustained transmission among cattle. [1-3] In January 2025, a second introduction of H5N1 encoding the clade 2.3.4.4b H5 HA but in the D1.1 genotype, was identified in dairy cattle and subsequently spread across multiple herds. [1] Viral RNA is detected in the milk and mammary tissue of dairy cattle, and experimental ingestion of contaminated milk in mice causes fatal systemic infection. [4,5] Ongoing transmission of HPAI H5N1 among dairy cattle and its spillover to other mammalian species increases the risk of human exposure and viral spread.

While there are currently no reports of HPAI H5N1 clade 2.3.4.4b in pregnant women from this outbreak, pregnant women have historically been at a greater risk of severe disease and death following infection with HPAI, as well as seasonal and pandemic influenza A viruses. [6,7] An analysis of 30 pregnant women diagnosed with avian influenza virus infection (H5N1, H5N6, and H7N9) reported that more than half (n=16) were infected with H5N1, which occurred across gestational ages, with all but two resulting in maternal and *in utero* fetal death. [6] Pregnant mice infected with H5N1 (A/Shenzhen/406H/2006) had detectable viral RNA in both placental and fetal tissues. [8] Despite poor maternal and infant outcomes, there is limited information on the pathogenesis of HPAI during pregnancy.

Pregnancy represents a distinct physiological and immunological state, which causes more severe outcomes from influenza infections than non-pregnant individuals. [6,7] The bovine H5N1 outbreak, including reports of fatal infections in cats on affected farms, [9] multiple infections among dairy farm workers, [10,11] and a pediatric H5N1 case, [12,13] emphasizes the public health risk and heightened potential for household exposure among pregnant women. Recent reports on cattle farms also indicate that H5N1-infected heifers exhibit reproductive complications, including abortions during mid- to late-gestation, and a reduced number of cattle in estrus during periods of high clinical disease. [14,15] While a previous study demonstrated that bovine H5N1 inoculation of post-birth lactating female mice can result in transmission of virus to offspring through milk, [4] it remains unknown whether *in utero* transmission of bovine H5N1 viruses occurs. To address this gap, we established a pregnancy mouse model to study the pathogenesis and transmission dynamics of bovine H5N1 from the 2024 outbreak. We intranasally inoculated pregnant CD-1 outbred mice at two gestational ages to investigate both *in utero* and post-birth transmission to offspring. Lastly, we evaluated the impact of maternal H5N1 infection on birth outcomes, neonatal growth, and postnatal neurodevelopment. Our study provides the groundwork for assessing H5N1 infection during pregnancy by establishing a pregnant mouse model and providing insights into viral dissemination and vertical transmission.

Results:

H5N1 dissemination and pathogenesis in non-pregnant and pregnant female mice

We examined the pathogenesis of two B3.13 genotype bovine isolates, A/bovine/Texas/98638/2024 (H5N1; A/bovine/TX) and A/bovine/Ohio/B24OSU-439/2024 (H5N1; A/bovine/OH) in non-pregnant outbred female mice. We utilized outbred mice because they better approximate the tolerogenic immune responses required to prevent rejection of semi-allogeneic fetuses, [16] and exhibit improved survival following pandemic H1N1 challenge compared with inbred strains. [16-18] We intranasally inoculated non-pregnant females with 100 TCID50 of A/bovine/TX, A/bovine/OH H5N1, or media. Similar morbidity was observed for

both viruses (**Figure 1A-B**). Peak clinical signs of disease appeared earlier in mice infected with A/bovine/TX (5 days post-infection [dpi]) compared to those infected with A/bovine/OH (9 dpi) (**Figure 1C**). All mice infected with A/bovine/TX succumbed by 6 dpi, while those infected with A/bovine/OH succumbed by 9 dpi (**Figure S1D**). At 5 dpi, females infected with A/bovine/TX exhibited greater infectious viral loads in the nasal turbinates, mammary glands, ovaries, and nervous system tissues (spinal cord, olfactory bulb, frontal lobe, and hindbrain) than females infected with A/bovine/OH (**Figure 1E**). Similar viral loads were detected in whole blood, trachea, lungs, and colon. We selected A/bovine/OH for subsequent experiments in pregnant mice to increase the probability of survival. When we infected non-pregnant mice with a lower dose of A/bovine/OH, although not statistically significant, mice infected with 10 TCID50 showed reduced morbidity and mortality compared to those infected with 100 TCID50 (**Figure 1F-G**).

To assess whether pregnancy increases morbidity and viral dissemination, we intranasally inoculated pregnant mice (dams) with either 10 or 100 TCID50 of A/bovine/OH at embryonic day (E)10, roughly corresponding to the human second trimester. [16,19] Rectal temperature indicated that the inoculation dose, more than pregnancy status, influenced morbidity (**Figure 2A**). Both pregnant and non-pregnant mice given 100 TCID50 showed greater hypothermia compared to those given 10 TCID50. At 6 dpi, non-pregnant females showed greater viral loads in both nasal turbinates and lungs. Pregnant mice, particularly those receiving 100 TCID50, showed greater detectable infectious virus in the ovaries and uterus (**Figure 2B**). Among females receiving the 100 TCID50 dose, infectious virus was detected in the ovaries and in at least one uterine horn in 6/6 pregnant mice, compared to infectious virus being detected in the ovaries and/or uterine horns of only 2/5 non-pregnant mice.

Histological examination of the lungs in the pregnant females infected with 100 TCID50 of A/bovine/OH revealed viral protein localized in luminal epithelial cells lining distal preterminal and terminal bronchioles and centriacinar alveoli (**Figure 2C**). Pulmonary histopathology was greater in pregnant mice infected with 100 TCID50 compared to those infected with 10 TCID50 or mock-infected (**Figure 2D**). While no histopathology was present in the lungs of mock-infected mice, there was moderate to severe pulmonary histopathology in infected mice, that was characterized by a locally extensive to widespread subacute necrotizing alveolitis and bronchiolitis (**Figure 2E**). Infected lungs had virus-induced apoptosis, necrosis, and exfoliation of airway epithelium lining distal, small-diameter bronchioles extending to terminal bronchioles in the centriacinar regions of the lung. Bronchiolar epithelial lesions were accompanied by an acute to subacute mixed inflammatory cell infiltrate composed of neutrophils and mononuclear cells (lymphocytes and monocytes) along with intramural and luminal accumulation of proteinaceous fluid (**Figure 2E, arrows**). Epithelial and inflammatory cell lesions extended into alveolar ducts and alveoli characterized by a necrotizing and exudative alveolitis with scattered focal areas of apoptotic epithelial cells and apoptotic bodies lining alveolar septa, and accumulation of mixed inflammatory cells and proteinaceous fluid in alveolar airspaces (**Figure 2E**). Although pregnancy does not increase morbidity during acute infection, it results in extensive pulmonary tissue damage and enhanced viral tropism in reproductive tissues.

In utero **vertical transmission of bovine H5N1**

To determine whether *in utero* vertical transmission occurred, placental and fetal tissues were examined for infectious virus at 6 dpi. Among pregnant females infected with 10 TCID50, 2/7 litters (11 of 42 conceptuses [comprising the uterus, placenta, and fetus]) had detectable infectious virus in the placenta, with one litter also showing corresponding viral detection in the

fetuses (4 of 42 conceptuses) (**Figure 3A**). Dams infected with 100 TCID50 had infectious virus detected in 6/6 litters (31 of 33 conceptuses), with three litters also exhibiting infectious virus in the fetuses (13 of 34 conceptuses), suggesting dose-dependent increased virus prevalence in the placenta and transmission to fetal tissues.

No histopathology was present in the placenta of mock-infected pregnant mice. For the embryonic age of the dams at the time of tissue collection (E16), there was an expected amount of degeneration and subsequent necrosis in the maternal decidua in mock dams and only slightly more decidual and junctional zone deterioration in H5N1-infected dams. In a subset of placentas from infected dams, virus-associated, small focal lesions were observed scattered within the labyrinth layer (**Figure 3B, arrows**). These lesions consisted of trophoblasts with nuclear inclusions or apoptotic cell death features, e.g., pyknosis, karyorrhexis, apoptotic bodies and phagocytic cells containing cellular debris. Virus-associated histopathological changes were observed in the columnar epithelial cells lining the yolk sac (**Figure 3C, arrows**).

Immunofluorescence staining for H5N1 antigen was utilized to identify the spatial distribution of the virus. No viral protein was observed in placentas collected from mock-infected dams (**Figure 3D**). Placentas from dams infected with 10 (**Figure S1A**) or 100 (**Figure 3E**) TCID50 displayed viral protein localized to the decidua, junctional zone, and labyrinth zone, consistent with the distribution of virus-associated lesions noted in the labyrinth zone. We evaluated the distribution of viral protein in fixed conceptuses to examine viral dissemination in tissues disrupted during the dissection process. Viral antigen was absent in the mock-infected dams (**Figure 3F**), but was detected in the yolk sac of a conceptus from one dam infected with 100 TCID50 (**Figure 3G**). Because the yolk sac plays a key role in fetal nutrition, [20] we evaluated placental and fetal mass at 6 dpi. Maternal H5N1 infection at E10 results in significantly decreased placental but not fetal mass (**Figure S1B-C**). Because infectious virus was detected in a subset of fetuses without growth restriction at either dose, we examined the localization of viral protein in fixed fetuses from litters that exhibited vertical transmission. This can provide a more comprehensive evaluation, as fetal orientation in fixed conceptuses can obscure the sagittal plane. Viral protein, absent in fetuses from mock-infected dams (**Figure 3H**), was localized in the intestinal tissue of fetuses from dams infected with either 10 (**Figure S1D**) or 100 (**Figure 3I**) TCID50.

Vertical transmission of bovine H5N1 post-birth

To investigate post-birth virus transmission, pregnant mice were inoculated with 10 or 100 TCID50 of A/bovine/OH during the human third trimester equivalent (E16). [16,19] Dams, along with their entire litter, were euthanized at 1 or 4 days post-birth (dpb), corresponding to 4 or 7 dpi. At 4 dpi (1 dpb), only 2/5 litters from dams infected with 100 TCID50 had detectable virus in at least one of the pups' lungs and /or milk ring, while virus was undetectable in all litters from dams infected with 10 TCID50 (**Figure 4A**). We evaluated viral dissemination in milk and four distinct mammary glands. [21] At 7 dpi (4 dpb), a subset of dams infected with 10 (3/6) or 100 (3/6) TCID50 had detectable virus in their lungs and mammary tissue (**Figure 4B**). Infectious virus was detected in at least one of the pups' lungs and/or milk ring from 1/6 dams infected with 10 TCID50 and 2/6 dams infected with 100 TCID50. Pups with detectable infectious virus were born to dams that also had virus detected in the milk and inguinal mammary tissue.

We determined whether the presence of H5N1 in mammary tissues resulted in pathological changes at 7 dpi (4 dpb). No histopathology was present in any of the lactating

mammary glands of mock-infected dams (**Figure 4C**). Terminal acinar lumens in the mock-infected dams contained a mixture of lipid and proteinaceous material, and the epithelial cells lining the lumens exhibited marked cytoplasmic vacuolation due to the presence of secretory lipid droplets. The terminal acinar lumens in the mammary glands of H5N1-infected dams were noticeably less distended, containing proteinaceous material, and exfoliated epithelial cells, with some cells exhibiting pyknotic or karyorrhectic nuclei (**Figure 4C, arrows**). Basophilic regenerative epithelium predominantly lined the acinar lumens of the H5N1-infected mice. When examining the presence of viral antigen by immunohistochemistry, cytoplasmic and nuclear staining of the N1 protein was observed in the epithelial cells lining the terminal acinar lumens for dams infected with either 10 (**Figure S2**) or 100 (**Figure 4C**) TCID50.

Compared to dams infected with 10 TCID50, those infected with 100 TCID50 exhibited increased morbidity, along with increased clinical signs of disease during the first week post-infection (**Figure 5A-B**). To further evaluate vertical transmission at later time points during lactation, dams were inoculated with 10 TCID50 A/bovine/OH at E16 to increase survival. Tissues from subsets of pups within individual litters were examined for infectious virus 1- 25 dpb, which corresponded to 4-28 dpi. Infected dams did not exhibit changes in morbidity, but clinical signs of disease peaked at 9 dpi (**Figure 5A-B**). Between 7 and 9 dpi, virus was detected in the lungs, mammary glands, and milk in a subset of dams (**Figure 5C**), whereas no virus was detected in tissues collected from dams euthanized at 28 dpi (**Figure 5D**). While no pups had detectable virus at 1 dpb (4 dpi), virus was detected in the milk ring, lungs, and blood from pups at 4 dpb (7 dpi) and 6 dpb (9 dpi) (**Figure 5E**). In contrast, no virus was detected in pups at either 12 dpb (15 dpi) or 25 dpb (28 dpi).

To confirm that dams and pups at 25 dpb (28 dpi) were infected, antibody responses to H5N1 were measured. H5- and N1-specific IgG and IgM titers were detectable in both dams euthanized at 28 dpi (**Figure 5F-H**). While the pups from the dams euthanized at 28 dpi did not have infectious virus, a subset of pups had detectable H5- and N1- specific IgG titers, suggesting either transfer of maternal antibodies or possible infection (**Figure 5F**). High titers of H5-specific IgG1, IgG2a, IgG2b, IgG2c, and IgG3 were detected in dams and pups, with N1-specific antibodies predominantly comprised of IgG2a, IgG2b, and IgG2c subclasses (**Figure S3**). Only one pup from each litter had detectable IgA (**Figure 5G**). Detectable H5- and N1-specific IgM were detected in one pup from each litter, suggesting a de novo immune response (**Figure 5H**). These data highlight that bovine H5N1 causes an acute infection in pregnant females and, at low doses, can lead to postnatal vertical transmission, which can be cleared from both the dam and fetuses.

Postnatal outcomes following maternal bovine H5N1 infection

To determine adverse developmental outcomes from maternal H5N1 infection, litters from pregnant females infected with either 10 or 100 TCID50 of A/bovine/OH at E16 were evaluated. Infection with either dose of H5N1 did not impact litter size (**Figure S4A**) or cause pre-term birth (**Figure S4B**). H5N1 infection of dams resulted in growth restriction in pups, as indicated by their smaller birth weight (**Figure 6A**), shorter body length (**Figure 6B**), and smaller head diameter (**Figure 6C**). Because dams infected with 100 TCID50 were euthanized by 7 dpi due to increased morbidity (**Figure 5A–B**), neurodevelopmental assessments were only conducted on pups from dams infected with 10 TCID50. At 5 dpb, cliff aversion (**Figure 6D**), measuring vestibular function, negative geotaxis (**Figure 6E**), measuring sensorimotor competence and vestibular function, and surface righting (**Figure 6F**), measuring motor development, were delayed in offspring of H5N1- compared to mock-infected dams and

continued until 9 dpb (**Figure 6G-I**). These results demonstrate that H5N1 infection in outbred dams during pregnancy results in both acute and persistent adverse perinatal and fetal outcomes, consistent with the intrauterine growth restriction observed in a human case of H5N1 infection [22].

Discussion:

We developed a model to study bovine H5N1 pathogenesis during pregnancy and observed distinct tissue tropism, with elevated viral titers in the reproductive tissues of pregnant mice. We showed *in utero* vertical H5N1 transmission following intranasal inoculation of outbred pregnant mice at E10, as indicated by infectious virus in placental and fetal tissues with viral protein localization in labyrinth zone, the yolk sac, and fetal intestines. Dams infected at E16 also transmitted virus to pups post-birth, most likely via milk, resulting in both acute and long-lasting adverse perinatal and developmental outcomes. These results provide insights into the vertical transmission dynamics of bovine H5N1 and contribute to the risk assessment of a high-risk population.

Infection during the second trimester (E10) of pregnancy reflects case studies that analyzed tissues from H5N1-positive patients. [6,23] We observed reduced placental mass with minimal placental pathology and no significant change in fetal mass. Analysis of a woman at 4 months of gestation who succumbed to H5N1 infection revealed normal placental development corresponding to gestational age and no histopathological abnormalities in fetal tissue. [23] Acute necrotizing deciduitis, also observed in our mouse model, was identified in the placenta of the pregnant woman. [23] Although placental and fetal damage was minimal, the woman exhibited widespread pulmonary damage, [23] consistent with our findings. When examining viral RNA or protein, the placental tissue from the pregnant woman showed infected cells in the chorionic villi, with viral RNA in the lungs and liver of the fetus. [23] We observed viral protein in the placental labyrinth zone. Both the mouse labyrinth and human chorionic villi are sites of maternal-fetal gas and nutrient exchange and are considered homologous structures. [24] Infection of inbred dams with A/Shenzhen/406H/2006 (clade 2.3.4) at E10 resulted in detectable viral RNA in both placental and fetal tissues with no analysis of anatomical distribution of virus. [8] In our model, viral protein was detected within the intestines of fetuses from H5N1-infected dams. We hypothesize fetuses may have ingested virus-containing amniotic fluid, which peaks during mid-to-late gestation and is critical for fetal intestinal development. [25] A previous human case of H5N1 infection during pregnancy reported intra-amniotic infection. [26] More recently, a study documented possible H5N1 vertical transmission during an HPAI H5N1 outbreak in South American sea lions, with placental lesions and viral RNA/protein detected in both placental and fetal tissues. [27] Cattle farms have also reported that H5N1-infected heifers exhibit reproductive complications, including abortions during mid- to late-gestation. [14,15] Investigating viral dissemination and mechanisms of H5N1 *in utero* vertical transmission using animal models has implications beyond human health, extending to other mammalian species, including livestock and marine mammals.

There are high levels of viral RNA or protein in milk and mammary tissue, accompanied by decreased milk production, and milk with a thickened, yellow-colored appearance in infected cattle. [9,28] Experimental intra-mammary infection in dairy cattle results in high viral loads in milk and infected udder quarters with limited local spread. [29,30] Viral antigen in the mammary tissue from inoculated quarters was detected in alveolar epithelial cells and was associated with alveolar shrinkage lined by swollen epithelial cells, and replacement of secretory alveoli with fibrous connective tissue. [29] This is consistent with our observation of viral antigen in the

epithelial cells lining the secretory alveoli of infected mammary tissue following intranasal inoculation. Whether these pathological changes are due to virus-induced pathology or a consequence of decreased milk production leading to mammary tissue reduction requires further study.

Given reports of fatal systemic influenza in cats and mice following ingestion of unpasteurized colostrum or milk from infected dairy cattle, [4,5,9] we also used this late-gestation infection model to investigate the transmission window of bovine H5N1 during lactation. Consistent with a previous study of H5N1 infected lactating BALB/c female mice, [4] we observed infectious virus in pups from infected pregnant mice at 7–9 dpi, corresponding to 4–6 dpb. Also consistent with the findings by Eisfeld et al., we observed detectable infectious virus in pups from 2 of 5 litters born to dams infected with 100 TCID50 at 7 dpi (4 dpb). [4] In addition to its influence on human health, our data contribute to understanding the agricultural impact, as H5N1 virus replication has been documented in the mouths of calves and can be transmitted to the mammary glands of lactating cattle. [31] Together, our results and those of previous studies further emphasize the importance of understanding virus transmission during lactation to prevent bidirectional H5N1 spread between lactating mothers and their offspring.

To date, no studies have examined offspring development following maternal H5N1 infection, whether acquired *in utero* or postnatally. We observed that H5N1 infection during pregnancy results in intrauterine growth restriction and offspring with neurodevelopmental delays, in the absence of pre-term birth or changes in litter size. Similar outcomes have been observed with H1N1 infection during pregnancy, resulting in adverse fetal outcomes in addition to long-term health effects, despite the absence of vertical transmission. [16,32] Therefore, it is imperative to investigate fetal outcomes in this bovine H5N1 vertical transmission model.

Mouse models of pregnancy are instrumental for uncovering mechanisms of disease pathogenesis and evaluating potential treatment options, particularly given the frequent exclusion of pregnant women from clinical trials. [33] While we established a mouse model of bovine H5N1 infection during pregnancy, we observed differences in morbidity and tissue tropism between two H5N1 clade B3.13 strains (A/bovine/TX and A/bovine/OH). These findings highlight the need for further studies to elucidate the pathogenesis of diverse H5N1 genotypes (e.g., B3.13 vs. D1.1). Analysis of virus replication and dissemination at multiple timepoints during acute infection during the second-trimester model (E10) would also provide greater insight into the pathogenesis of H5N1. It is also unclear what selective pressure transmission via milk has on the virus itself, as this may differ significantly from selective pressure in the lungs or placentas. Evaluating changes in virus sequences in infected milk and in pups infected with virus-containing milk could help inform whether vertical transmission can lead to more efficient mammalian adaptation of H5N1 viruses.

H5N1 clade 2.3.4.4b has spread among numerous placental mammals, heightening concerns about their zoonotic potential amid repeated introductions to dairy cattle. In addition to the infections in barn cats [9] on affected farms and multiple infected dairy farm workers, [10] a recent report documented H5N1 infection in indoor domestic cats from households of dairy workers employed on farms positive for H5N1 (genotype B3.13). [34] Although the current public health risk of H5N1 remains low, potential exposure and transmission, such as fomites, from individuals working with infected cattle or poultry to household pets and family members is possible. These results provide the groundwork for understanding the vertical transmission of bovine H5N1 viruses in humans and other placental mammals, including cattle, where adverse pregnancy outcomes have recently been reported following H5N1 infection. [14,15]

Resource Availability:

Lead Contact

Further information and requests for resources should be addressed to the lead contact, Sabra L. Klein (sklein2@jhu.edu)

Materials availability:

Materials used in this study are available from the lead contact.

Data and Code availability:

All data are available in the main text or the supplementary materials.

Acknowledgments:

We are grateful for the animal care staff that assisted with animals from the Miller Research Building Animal Facilities at Johns Hopkins University. Light microscopy images were generated using the instruments and support of the Light Microscopy Core of the Department of Molecular Microbiology and Immunology at the Johns Hopkins Bloomberg School of Public Health. We are also thankful for the histology laboratory personnel at the Johns Hopkins Oncology Tissue Services, and the Klein, Davis, and Thompson lab members for discussions about these data. We would also like to acknowledge Ryan Lewandowski for his technical assistance of digital histology scans at Michigan State University. Funding was provided by the National Institutes of Health, NIAID Johns Hopkins Center of Excellence for Influenza Research and Response (75N93021C00045; AP and SK), NIH/NIAID F32HD117584 (BS), and the NIH/NIAID 5T32AI007417-29 (MP).

Author contributions:

Conceptualization: BAS, MAP, AP, SLK

Methodology: BAS, LC, ASB, RJW, JRH, AP, SLK

Investigation: BAS, MAP, SNT, TZ, SC, JAL, JS

Visualization: BAS, JRH

Funding acquisition: SLK, AP

Project administration: SLK

Supervision: JRH, AP, SLK

Writing – original draft: BAS, JRH, AP, SLK

Writing – review & editing: All authors

Declaration of interests:

Authors declare that they have no competing interests.

Main Figure Titles and Legends:

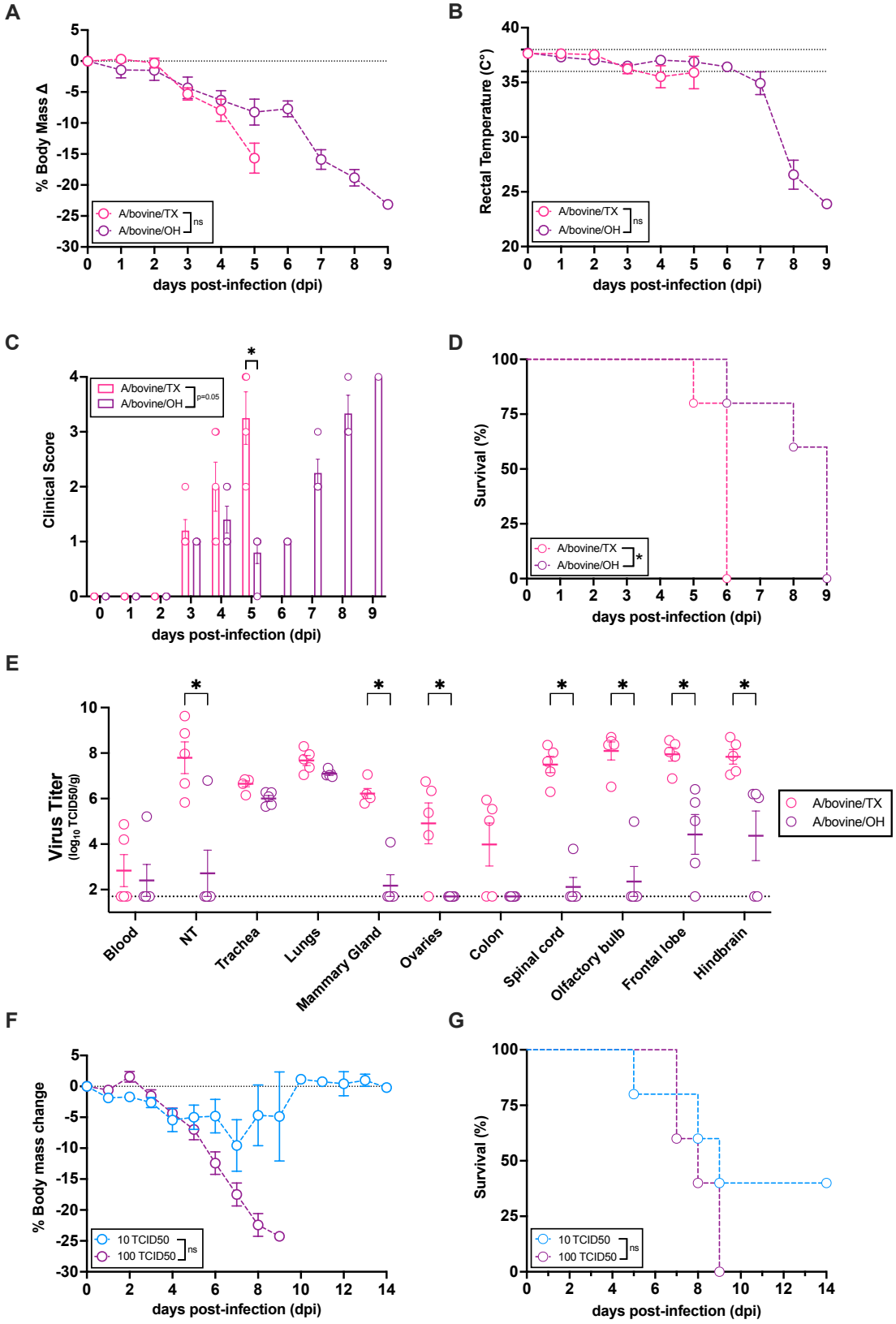

Figure 1. Pathogenicity of bovine H5N1 virus in nonpregnant female CD-1 mice. CD-1 female mice (7-8 weeks of age, n=5 per group) were intranasally inoculated with 100 TCID50 of A/bovine/Texas/98638/2024 (H5N1; A/bovine/TX) or A/bovine/Ohio/B24OSU-439/2024 (H5N1; A/bovine/OH). (**A**) Body mass and (**B**) rectal temperature were recorded daily as a measure of morbidity. (**C**) Clinical scores, including dyspnea, piloerection, hunched posture, and absence of an escape response, were documented daily and quantified on a scale of 0 - 4. (**D**) Survival was recorded daily. (**E**) At 5 days post-infection, mice inoculated with A/bovine/TX or A/bovine/OH (7-8 weeks of age, n=5 per group) were euthanized and tissues were collected for viral quantification by TCID50 assay. **(F, G)** CD-1 female mice (7-8 weeks of age, n=5 per group) were inoculated with 10 or 100 TCID50 of A/bovine/OH and (**F**) body mass and (**G**) survival were monitored daily for 14 days. Individual symbols (A and B, F and G) or bars (C) represent the mean ± standard error of the mean per group, with individual mice indicated by symbols in (E). Significant differences ($p < 0.05$) were determined by performing a two-tailed unpaired t-test of the calculated area under the curve (A-C, F-G), multiple unpaired t-test (C), Mantel-Cox (D), or a two-way ANOVA with Bonferroni post-hoc test (E) and are indicated by an asterisk (*).

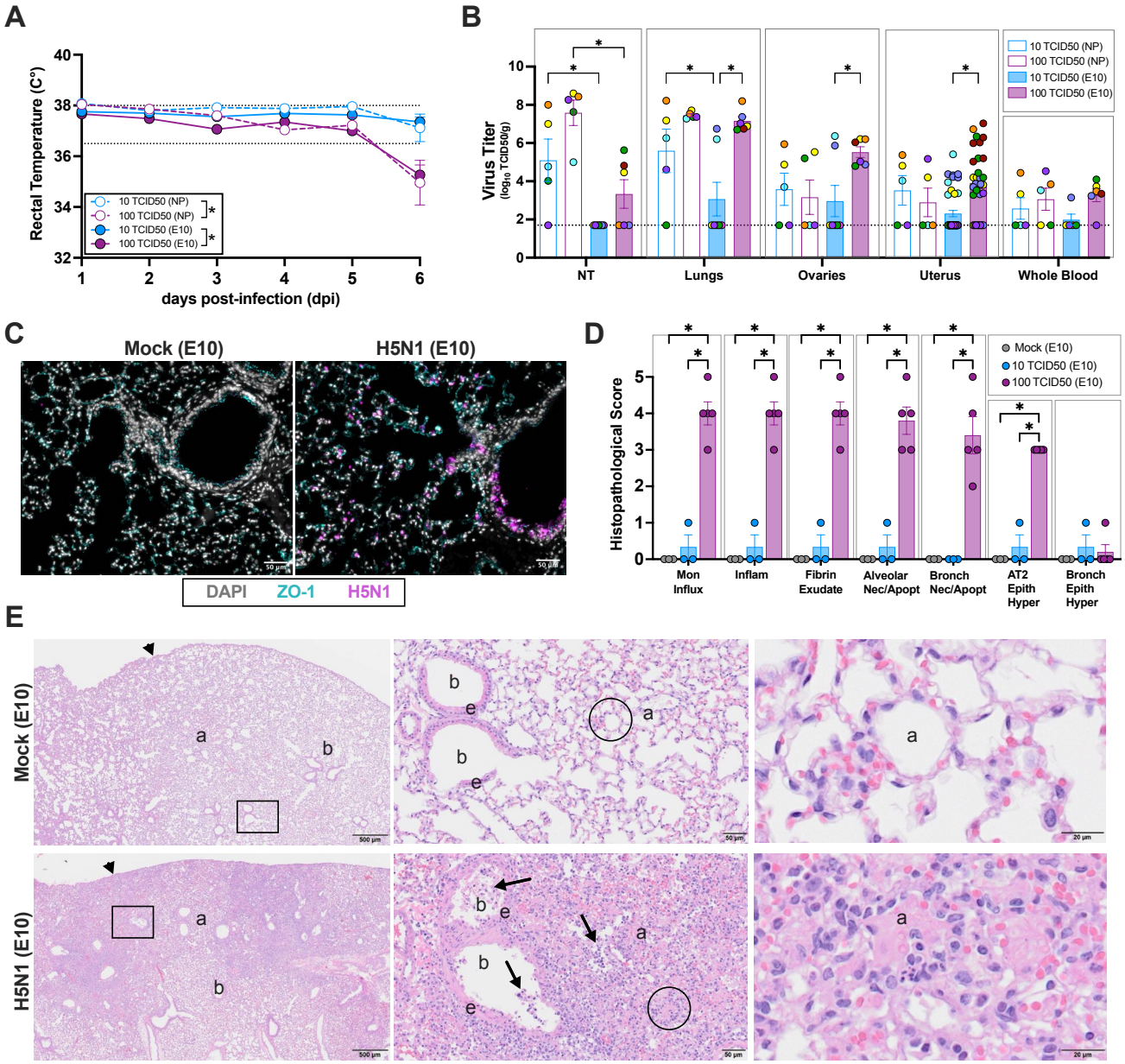

Figure 2. Pathogenesis of bovine H5N1 in non-pregnant and pregnant (second-trimester equivalent gestation) female mice. CD-1 non-pregnant (7-8 weeks of age; n=5 per group) or pregnant (embryonic day 10; n=6-7 per group) female mice were intranasally inoculated with 10 or 100 TCID50 of H5N1 (A/bovine/OH). Mock controls were inoculated with media alone. (**A**) Rectal temperature was recorded daily as a measure of morbidity. The dashed line represents the rectal temperature range for a healthy mouse. (**B-E**) At 6 days post-infection, a subset of mice (n=5-7) from each group were euthanized and tissues were collected for downstream analysis. (**B**) Infectious virus was quantified by TCID50 assay in the nasal turbinates, lungs, ovaries, and whole blood of non-pregnant and pregnant dams. Individual points are color-coded by animal, while bar colors indicate group. (**C**) Immunofluorescent staining of fixed lung tissue (mock – left, and 100 TCID50 – right) from E10 pregnant dams. Cell nuclei (DAPI) are labeled in grey, tight junctions (ZO-1) are labeled in cyan to distinguish structural features, and H5N1 virus protein is labeled in magenta. The scale bar is located in the bottom right corner at 50 µm. (**D**) Severity of individual

lesions (histopathology) in lung tissue from E10 pregnant dams was scored by a board-certified pathologist for monocyte influx (Mon Influx), inflammation (Inflam), fibrin exudate, alveolar necrosis and apoptosis (Alv Necr Apopt), bronchiolar necrosis/apoptosis (Bronch Necr/Apopt), AT2 epithelial hyperplasia (AT2 Epith Hyper), and bronchiolar epithelial hyperplasia (Bronch Epith Hyper). (**E**) Light photomicrographs of hematoxylin and eosin–stained lung tissue taken at three different magnifications (low (scale bar: 500 µm), medium (scale bar: 50 µm) and high (scale bar: 20 µm)) from right to left, respectively. Squares and circles indicate the location of magnified images to the right. Arrows in the lower middle photo highlight virus-induced inflammatory cell exudate in airway and alveolar airspaces─a, alveoli and b, bronchiole. Arrows in the right lower photo highlight the presence of apoptotic epithelial cells and apoptotic bodies lining alveolar septa, with accumulation of mixed inflammatory cells and proteinaceous fluid in alveolar lumens. Individual symbols (A) or bars (B and D) represent the mean ± standard error of the mean per group, with individual mice indicated by the color-coded points (B and D). Significant differences ($p < 0.05$) were determined by a repeated measures two-way ANOVA with Bonferroni post-hoc test (A) or two-way ANOVA with Bonferroni post-hoc test (B and D) and are indicated by an asterisk (*).

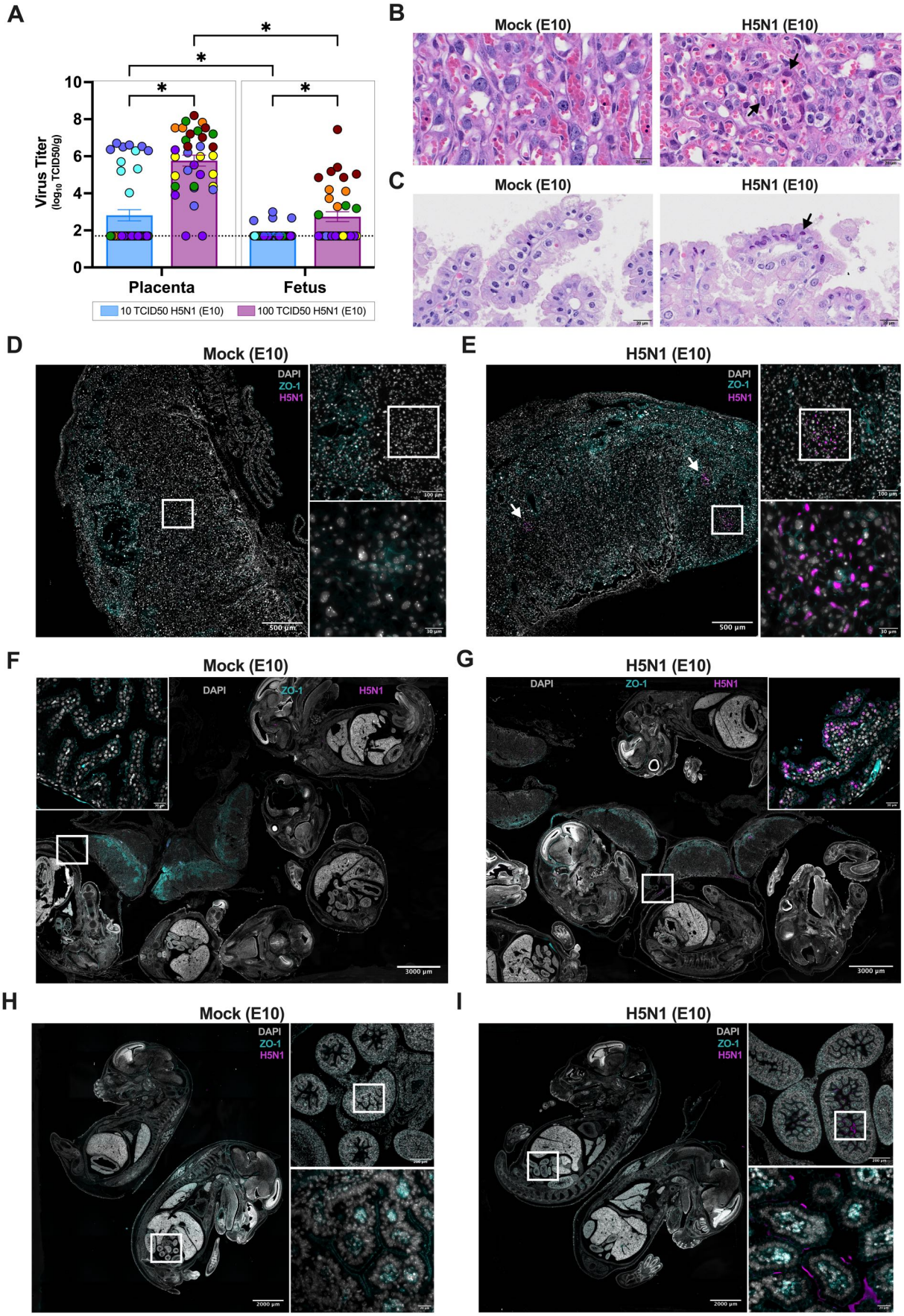
A
Virus Titer
(log10 TCID50/g)
10
8
6
4
2
0
*
*
*
*
Placenta
Fetus
10 TCID50 H5N1 (E10)
100 TCID50 H5N1 (E10)
B
Mock (E10)
H5N1 (E10)
C
Mock (E10)
H5N1 (E10)
D
Mock (E10)
DAPI
ZO-1
H5N1
500 µm
E
H5N1 (E10)
DAPI
ZO-1
H5N1
500 µm
F
Mock (E10)
DAPI
ZO-1
H5N1
3000 µm
G
H5N1 (E10)
DAPI
ZO-1
H5N1
3000 µm
H
Mock (E10)
DAPI
ZO-1
H5N1
2000 µm
I
H5N1 (E10)
DAPI
ZO-1
H5N1
2000 µm

Figure 3. *In utero* vertical transmission and conceptus tissue tropism of bovine H5N1. CD-1 pregnant (embryonic day [E] 10) dams were intranasally inoculated with media, 10 TCID50, or 100 TCID50 of H5N1 (A/bovine/OH). (**A**) At 6 days post-infection, a subset of mice (n= 5-7) from each group were euthanized, and infectious virus was quantified by TCID50 assay in a subset of placental and fetal tissues (n= 4-6/dam). The dashed line indicates the limit of detection. Individual points are color-coded by litter corresponding to the color of the dam in Fig. 1, while bar colors indicate viral dose. (**B, C**) Hematoxylin and eosin–stained placental tissue from E10 pregnant dams. The scale bar is located in the bottom right corner at 20 µm. (**B**) Placental labyrinth of pregnant dams that were mock infected (controls) or inoculated with H5N1 (100 TCID50). (**C**) Yolk sac from pregnant dams mock infected or inoculated with H5N1 (10 TCID50). Arrows represent virus-associated, small focal lesions. Immunofluorescent staining of the (**D–E**) placenta, (**H-I**) conceptus, and (**F–G**) fetus from E10 pregnant dams inoculated with (**D, H, F**) media or (**E, G, I**) H5N1 (100 TCID50). The left images were taken at (**D**) 4X (scale bar: 500 µm) or (**F-H**) 4X tiled images (scale bar: 2,000 or 3,000 µm). Higher-resolution images were captured at (**D** and **E**; top right) 20X (scale bar: 100 µm) or (**H** and **I**; top right) 10X (scale bar: 200 µm) and/or (**D-E** and **H-I**; bottom right) 60X (scale bar: 20 or 30 µm). The small panel in **F-G** was captured at 40X (scale bar: 30 µm). White boxes indicate the regions displayed in the magnified images. Cell nuclei (DAPI) are shown in grey, tight junctions (ZO-1) in cyan to distinguish structural features, and H5N1 whole virus antigen in magenta. Bars (A) represent the mean ± standard error of the mean per group, with individual mice indicated by colored points. Significant differences ($p < 0.05$) were determined by a two-way ANOVA with Bonferroni post-hoc test (A-B) and are indicated by an asterisk (*).

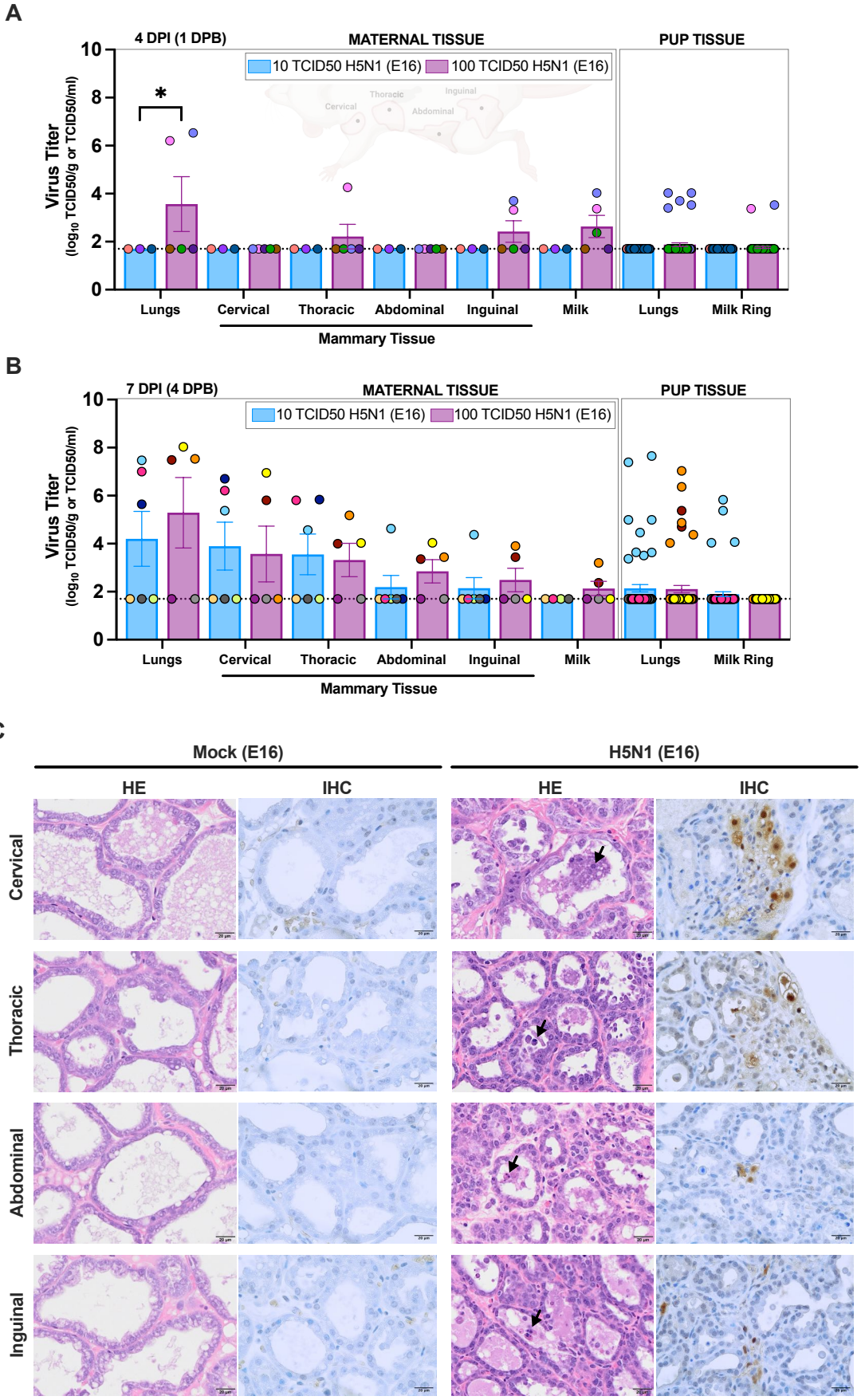
A
4 DPI (1 DPB)
MATERNAL TISSUE
PUP TISSUE
10 TCID50 H5N1 (E16)
100 TCID50 H5N1 (E16)
Virus Titer
(log10 TCID50/g or TCID50/ml)
*
Lungs
Cervical
Thoracic
Abdominal
Inguinal
Milk
Lungs
Milk Ring
Mammary Tissue
B
7 DPI (4 DPB)
MATERNAL TISSUE
PUP TISSUE
10 TCID50 H5N1 (E16)
100 TCID50 H5N1 (E16)
Virus Titer
(log10 TCID50/g or TCID50/ml)
Lungs
Cervical
Thoracic
Abdominal
Inguinal
Milk
Lungs
Milk Ring
Mammary Tissue
C
Mock (E16)
H5N1 (E16)
HE
IHC
HE
IHC
Cervical
Thoracic
Abdominal
Inguinal

Figure 4. Post-birth vertical transmission and tissue tropism of bovine H5N1. CD-1 pregnant (embryonic day [E] 16) females were intranasally inoculated with 10 or 100 TCID50 of H5N1 (A/bovine/OH). At (**A**) 4 days post-infection (1-day post-birth) or (**B**) 7 days post-infection (4 days post-birth), a subset of dams and their entire litters were euthanized. Infectious virus was quantified by TCID50 assay in the lungs, milk, and mammary tissue (cervical, thoracic, abdominal, and inguinal) of lactating dams, as well as in the pup lungs and milk ring. The pregnant dam infected with 10 TCID50 succumbed to the infection just before sample collection; therefore, milk was not available for virus titration. Individual points are color-coded by litter. (**C**) Hematoxylin and eosin–stained mammary tissue sections collected 7-8 dpi from E16 pregnant dams (mock – left and 100 TCID50 – right). Arrows indicate pyknotic or karyorrhectic nuclei. Immunohistochemistry staining for viral N1 antigen of fixed cervical, thoracic, abdominal, and inguinal mammary tissue (mock – left, and 100 TCID50 – right). The scale bar is located in the bottom right corner at 20 µm. Illustration depicting the collection sites for the various mammary glands was created in BioRender. Seibert, B. (2025) https://BioRender.com/tq8un5s. Bars (A-B) represent the mean ± standard error of the mean per group. Significant differences ($p < 0.05$) were determined by a two-way ANOVA with Bonferroni post-hoc test (A-B) and are indicated by an asterisk (*).

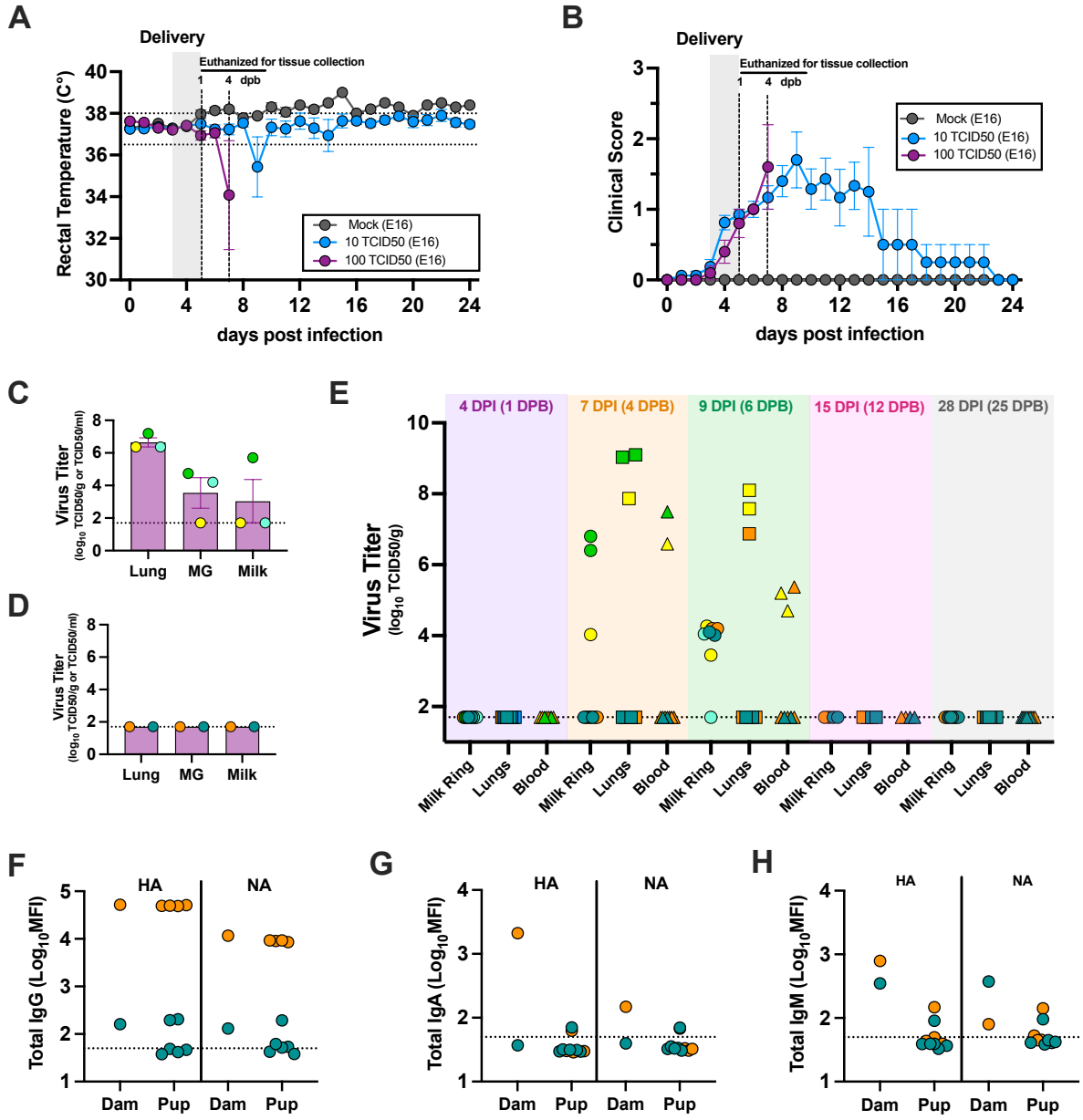

Figure 5. Post-birth bovine H5N1 virus transmission dynamics to offspring. CD-1 pregnant dams (embryonic day 16) were intranasally inoculated with media or 10 or 100 TCID50 of H5N1 (A/bovine/OH). (**A**) Rectal temperature was recorded daily as a measure of morbidity. The dashed line represents the rectal temperature range for a healthy mouse. (**B**) Clinical scores, including dyspnea, piloerection, hunched posture, and absence of an escape response, were documented daily and quantified on a scale of 0 - 4. The shaded grey bar marks the time of delivery. Dams inoculated with 100 TCID50 were euthanized at 4 or 7 days post-infection (dpi), indicated by a dashed line, while a separate group of mock-infected and 10 TCID50 infected dams were monitored up to 24 days post-infection. Between (**C**) 4-6 and (**D**) 28 dpi, a subset of dams (n=2-3/dpi) inoculated with media or 10 TCID50 of H5N1 (A/bovine/OH) were euthanized, and infectious virus was quantified by TCID50 assay in the lungs, mammary glands (MG), and milk. The dashed line indicates the limit of detection. (**E**) A subset of pups (n= 4-10/ days post-birth (dpb)) was euthanized at 4 days dpi (1 dpb), 7 dpi (4 dpb), 9 dpi (6 dpb), 15 dpi (12 dpb), and 28

dpi (25 dpb) and tissues, including the milk ring, lung, and whole blood, were collected and analyzed for infectious virus by TCID50 assay. The dashed line indicates the limit of detection. H5N1 HA and NA specific (**F**) IgG, (**G**) IgA, and (**H**) IgM were measured in serum from dams and their corresponding pups euthanized at 28 dpi (25 dpb) using systems serology. The results are reported as $\log_{10}$ mean fluorescence intensity (MFI). The dashed line indicates the limit of assay background. Individual points are color-coded by individual dam and their corresponding pups. Individual points (A-B) or bars (C-D) represent the mean ± standard error of the mean per group.

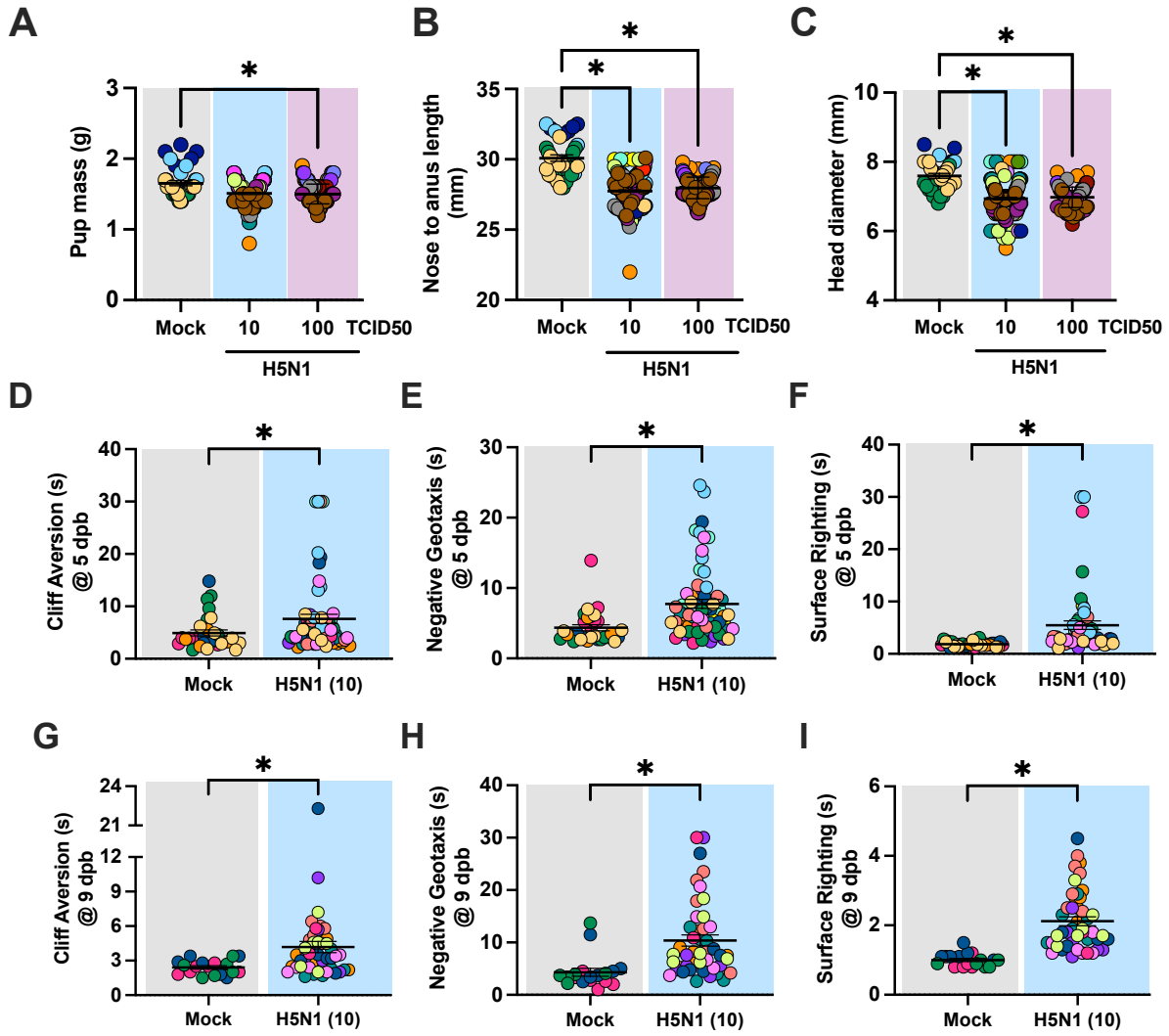

Figure 6. Perinatal outcomes following bovine H5N1 virus infection during the third-trimester gestation. CD-1 pregnant (embryonic day 16) dams were intranasally inoculated with media or 10 or 100 TCID50 of H5N1 (A/bovine/OH). Within the first 12 hours of birth, (**A**) body mass, (**B**) length measured from nose to anus, (**C**) and head diameter of each pup were measured. At 5 (**D-F**) and 9 (**G-I**) dpb, a subset of pups from each litter was assessed for cliff aversion (D and G), negative geotaxis (E and H), and surface righting (F and I) to measure neurological development. Individual points are color-coded by litter, while shaded colors indicate group: grey for media, blue for 10, and purple for 100 TCID50-inoculated pregnant dams. Horizontal bars indicate mean values across samples with bars indicating standard error of the mean for each group. Significant differences ($p < 0.05$) were determined by a two-tailed unpaired t-test and are indicated by an asterisk (*).

Methods:

EXPERIMENTAL MODEL DETAILS

Animal experiments

Adult (8–12 weeks of age), non-pregnant female or timed-pregnant CD-1 mice were purchased from Charles River Laboratories. Pregnant mice were received on embryonic day (E) 8 or E14. Five non-pregnant female mice were housed per cage, while each pregnant mouse was singly housed. Mice were housed under standard animal biosafety level 3 (ABSL3) housing conditions with *ad libitum* food and water in the ABSL3 facility at the Johns Hopkins School of Medicine. Mice were given at least 24 hours to acclimate to the ABSL3 facility before infection [16]. All monitoring and experimental procedures were consistently performed at the same time each day. Studies were conducted under Biosafety Level 3 (BSL-3) containment and approved by Johns Hopkins University Animal Care and Use Committee (ACUC; Protocol MO24H150).

Cells

Madin-Darby canine kidney (MDCK) cells, a kind gift from Dr. Robert A. Lamb, were maintained in complete medium (CM) consisting of Dulbecco's Modified Eagle Medium (DMEM, Sigma-Aldrich, St Louis, MO, USA) supplemented with 10% fetal bovine serum (FBS; Gibco, Waltham, MA, USA), 100 units/ml penicillin/streptomycin (Life Technologies, Frederick, MD, USA) and 2 mM Glutamax (Gibco, Waltham, MA, USA) at 37 °C and 5% CO2.

Viruses

The viruses utilized in this study: A/bovine/Texas/98638/2024 (H5N1; A/bovine/TX) and A/bovine/Ohio/B24OSU-439/2024 (H5N1; A/bovine/OH) were kindly provided by Dr. Andrew Bowman (The Ohio State University, Columbus, OH, USA) and Dr. Richard Webby (St Jude Children's Research Hospital, Memphis, TN, USA). [35] Virus stocks of A/bovine/TX and A/bovine/OH were generated by infecting Madin-Darby canine kidney (MDCK) cells at a multiplicity of infection (MOI) of 0.01 infectious units per cell, at 33°C using infection media (CM with no FBS and 5 µg/ml of N-acetyl Trypsin) as previously described. [36]

METHOD DETAILS

Inoculation and monitoring of mice

Mice were anesthetized via intraperitoneal injection of a ketamine/xylazine cocktail (80 mg/kg ketamine, 5 mg/kg xylazine) prior to inoculation. Mice were intranasally inoculated with either 10 or 100 TCID50 of A/bovine/Texas or A/bovine/Ohio in 30µL of DMEM. Following intranasal inoculation, body mass, rectal temperature, and appearance of clinical signs were recorded once daily in the morning until tissue collection (4-28 days post-infection [dpi]). Clinical scores were reported on a scale of 0–4, with 1 point assigned for each of the following: piloerection, dyspnea, hunched posture, and absence of an escape response, on each day. [37,38]

Milk collection from lactating mice

Lactating dams were separated from their litters for at least 30 min to allow milk accumulation. Mice were then anesthetized via intraperitoneal injection of a ketamine/xylazine cocktail (80 mg/kg ketamine, 5 mg/kg xylazine) followed by intraperitoneal injection of oxytocin acetate salt

hydrate (0.05 mg/kg; Sigma-Aldrich, St Louis, MO, USA) to stimulate milk production. Milk was then expressed from the teat through manual stimulation and collected using a pipette, as previously described. [39] Milk was pooled from all teats during the collection process.

Tissue and serum collection from mice

Experimental pregnant and non-pregnant female mice were euthanized via ketamine/xylazine overdose (160 mg/kg ketamine, 10 mg/kg xylazine) followed by cardiac exsanguination. For dams infected at E10, tissues were collected at 6 dpi. For dams infected at E16, tissues were collected at 4, 7, 9, 15, and 28 dpi, unless dams succumbed to infection prior to the assigned collection date, then tissues were flash-frozen on dry ice one day prior. Half of the whole blood was saved for virus titration, while the remaining volume was centrifuged at 10,000 × g for 30 minutes at 4°C to separate the serum. For the collection of reproductive tissues in pregnant mice, the uterine horns were removed, and every other conceptus starting at the top of the left uterine horn was flash frozen (the placenta, fetus, and uterine tissue were separated and frozen individually). This was performed until a total of 6 of each tissue were collected per dam. For tissues collected from pups after birth, pups were anesthetized via isoflurane and euthanized via decapitation. Tissues were collected and flash-frozen on dry ice at the specified time points post-birth.

Offspring measurements and developmental assessments

Gestational age of delivery, litter size, and offspring from mock and H5N1-infected dams were measured within the first 12 h of birth. Measurements including pup mass (g), head size measured as ear-to-ear diameter (mm), and length defined as nose to anus (mm) were recorded for each pup. At 5 and 9 days after birth, a subset of pups was subjected to neurodevelopmental tests, including cliff aversion, negative geotaxis, and surface righting, as previously described. [7,16,40] For each test, at least 2 males and 2 females were used to limit confounding litter effects. Each pup performed each test three times, and the best time was recorded for each. Tests were considered failed and assigned a time of 30 seconds if the task was not completed. For cliff aversion testing, pups were briefly placed with their forepaws on the edge of a box, and the latency to retreat from the ledge was recorded. Negative geotaxis was assessed by placing pups facing downward on a 45° incline and recording the time taken to rotate 180° to face upward. Surface righting was assessed by recording the time required for a pup to turn from a prone to an upright position.

Virus Titration

Frozen tissues were thawed and placed into Lysing Matrix D tubes (MP Biomedicals, Santa Ana, CA, USA) with homogenization media (500mL DMEM, 5mL penicillin/streptomycin) with a minimum volume of 400µL and a maximum volume of 1200µL (10% weight/volume). Tissues were homogenized at 4.0 m/s for 45 seconds in a MP Fast-prep 24 5G instrument (MP Biomedicals, Santa Ana, CA, USA and centrifuged at 500 *g* for 5 minutes. Supernatants were collected, aliquoted, and stored at –80°C until further analysis. The supernatant from tissue homogenates was titrated by TCID50 assay using the Reed and Muench method. [36,41]

Histopathology

Selected tissues, including lungs, placentas, fetuses, conceptuses, and mammary tissues were collected and fixed in formalin (Z-FIX, Fisher Scientific, Waltham, MA, USA) for histopathological examination. Prior to fixation, the left lung was perfused with formalin. Conceptuses remaining after flash-freezing tissues for viral titration were fixed, with the

placenta, fetus, and uterine tissue dissected and fixed individually, beginning at the top of the left uterine horn. When there were more than 12 conceptuses, whole conceptuses (fetal, placental, and uterine tissue) were fixed without separation of individual tissues. Tissues were fixed for at least 72 hours prior to paraffin embedding and processing for routine histopathology with hematoxylin and eosin staining (H&E). A board-certified pathologist, blinded to the study, subjectively scored tissues (n=3 mocks, n=4 10 TCID50, n=6 100 TCID50) as follows: (0) none; (1) mild; (2) mild to moderate; (3) moderate; (4) moderate to severe; (5) severe.

Immunohistochemistry

An antibody targeting influenza A virus N1 (Goat; Polyclonal Anti-Influenza Virus N1 Neuraminidase (NA), A/New Jersey/8/1976 (H1N1), BEI Resources, Manassas, VA, USA; RRID: AB_3711611; dilution 1:250) was used to perform immunohistochemistry on mammary sections. Briefly, tissues embedded in paraffin were dewaxed according to an established protocol, [42] and antigen retrieval was performed by incubating slides in citrate buffer (Abcam; Cambridge, UK) within a steamer for 45 minutes. Tissues were then blocked with 3% hydrogen peroxide for 10 min, permeabilized with PBS-Triton (0.3%), and then blocked with normal donkey serum (Jackson ImmunoResearch, West Grove, PA, USA; 10%) and bovine serum albumin (BSA; 1%) for 2 hours at room temperature. Slides were incubated overnight at 4°C with the primary antibody diluted in 3% BSA, followed by washing with 0.1% PBS-Tween and incubation with Donkey anti-Goat IgG (H+L) Secondary Antibody, HRP (ThermoFisher, Waltham, MA, USA; RRID:AB_2534673; 1:500 dilution) for 1 hour at room temperature. Antibody binding was visualized using DAB (3,3′-diaminobenzidine; Vector Laboratories, Newark, California, USA) as the chromogen following the manufacturer's instructions.

Immunofluorescence

As in the immunohistochemistry protocol, paraffin-embedded tissues were dewaxed and subjected to antigen retrieval. Tissues were then permeabilized with PBS-Triton (0.3%), stained using TrueBlack Lipofuscin Autofluorescence Quencher in DMF (biotium, Fremont, CA, USA), and then blocked with normal goat serum (NGS; Jackson ImmunoResearch, West Grove, PA, USA; 5%) for 1 hour at room temperature. Slides were incubated overnight at 4°C with primary antibodies targeting ZO-1 (Mouse; ZO-1 Monoclonal Antibody (ZO1-1A12), ThermoFisher,Waltham, MA, USA; RRID:AB_2533147; dilution 1:200) and H5N1 (Rabbit; Rabbit Anti-H5 Serum Control Panel; BEI Resources, Manassas, VA, USA; RRID: AB_3711610; dilution 1:200) diluted in 3% NGS, followed by washing with 0.1% PBS-Tween and incubation with Goat anti-Mouse IgG (H+L) Cross-Adsorbed Secondary Antibody, Alexa Fluor™ 488 (ThermoFisher, Waltham, MA, USA; RRID:AB_2534069; dilution 1:1000) and Goat anti-Rabbit IgG (H+L) Cross-Adsorbed Secondary Antibody, Alexa Fluor™ 555 (ThermoFisher, Waltham, MA, USA; RRID:AB_2535849; dilution 1:1000) for 2 hours at room temperature. Tissues were subsequently incubated with DAPI (ThermoFisher, Waltham, MA, USA; 1 μg/mL) for 4 minutes, as per the manufacturer's instructions. Tissues were imaged using a Nikon Eclipse Ti2-E microscope (Nikon, Minato City, Tokyo, Japan) and then further processed in ImageJ [43].

Luminex Serological Assays

Antibodies were measured through multiplex Luminex serological assays as previously described. [44] Antigens used for these analyses include Influenza A H5N1 (A/Texas/37/2024), A/dairy cow/Texas/24-008749-002-v/2024 Hemagglutinin HA Protein (SinoBiological, Beijing, China), and the bovine N1 construct was kindly provided by Lynda Coughlan (University of

Maryland, MD, USA) and produced in Expi293F cells as previously described. [45] Each antigen was coupled to unique MagPlex bead regions (Luminex). Briefly, beads were activated by combining activation buffer (0.1M NaH2PO4; pH 6.2), 50mg/mL 1-ethyl-3-[3-dimethylaminopropyl] carbodiimide (EDC), and 50mg/mL Sulfo-NHS (N-hydroxysulfosuccinimide). Activated beads were coupled to 25 µg of antigen in coupling buffer (0.05 M MES, pH 5.0). Activated coupled beads were blocked with blocking buffer (PBS 1X, 0.1% BSA, 0.02% Tween-20, 0.05% sodium azide; pH 7.4), washed with washing buffer (PBS 1X, 0.05% Tween-20) and stored at 4°C in PBS. To measure immunoglobulin isotypes, serum was heat-inactivated at 56°C for 30min and diluted 1:25 in PBS. 5µL of diluted serum run in duplicate was incubated with 45µL of bead solution (20µL of each bead region in 20µL Luminex Assay Buffer per plate) in a 384-well plate format for 2 hours shaking at 750 rpm. Following incubation, the plates were washed three times with Procartaplex Wash Buffer. Isotypes were identified by 1 hour incubation shaking at 750rpm with 45µL of PE-conjugated isotype-specific antibody (Southern Biotech, Homewood AL, USA; IgG RRID:AB_2794298; IgG1 RRID:AB_2794434; IgG2a RRID:AB_2794502; IgG2b RRID:AB_2756437; IgG2c RRID:AB_2794468; IgG3 RRID:AB_2794576; IgM RRID:AB_2794265; IgA RRID:AB_2794375). Following final incubation, the plates were washed three times with Procartaplex Wash Buffer and resuspended in 50µL of Procartaplex Wash Buffer for reading on the Luminex Intelliflex. Samples were run on FlexMap 3D Low with a DD range of 7000-1700. For each assay, a minimum of 100 events was recorded per antigen and the MFI of secondary antibody-conjugated to PE for each bead region was measured to quantify antigen-specific immunoglobulin isotype responses in each sample. Limit of background (LOB) was set by the PBS negative control.

Statistical Analyses

Statistical analyses were performed using GraphPad Prism v10.3.1 for Mac, GraphPad Software, Boston, Massachusetts, USA, www.graphpad.com. Kaplan-Meier curves were compared using the log-rank Mantel-Cox test. The area under the curve (AUC) of body mass change and rectal temperature curves was analyzed by a two-tailed unpaired t-test. Cumulative clinical scores were analyzed using the Kruskal-Wallis test. Viral titers, antibody measures, pup measurements, and developmental tests were analyzed using 1-way or 2-way ANOVAs followed by post hoc Bonferroni multiple comparisons test. Mean or median differences were considered statistically significant at $P < 0.05$ and are represented by a single asterisk.

References and Notes

1. Lowen, A.C., Baker, A.L., Bowman, A.S., Garcia-Sastre, A., Hensley, S.E., Lakdawala, S.S., Moncla, L.H., Nelson, M.I., Pekosz, A., Poulson, R.L., et al. (2025). Pandemic risk stemming from the bovine H5N1 outbreak: an account of the knowns and unknowns. J Virol *99*, e0005225. 10.1128/jvi.00052-25.
2. Nguyen, T.Q., Hutter, C.R., Markin, A., Thomas, M., Lantz, K., Killian, M.L., Janzen, G.M., Vijendran, S., Wagle, S., Inderski, B., et al. (2025). Emergence and interstate spread of highly pathogenic avian influenza A(H5N1) in dairy cattle in the United States. Science *388*, eadq0900. 10.1126/science.adq0900.
3. Mostafa, A., Nogales, A., and Martinez-Sobrido, L. (2025). Highly pathogenic avian influenza H5N1 in the United States: recent incursions and spillover to cattle. Npj Viruses *3*, 54. 10.1038/s44298-025-00138-5.
4. Eisfeld, A.J., Biswas, A., Guan, L., Gu, C., Maemura, T., Trifkovic, S., Wang, T., Babujee, L., Dahn, R., Halfmann, P.J., et al. (2024). Pathogenicity and transmissibility of bovine H5N1 influenza virus. Nature *633*, 426-432. 10.1038/s41586-024-07766-6.
5. Guan, L., Eisfeld, A.J., Pattinson, D., Gu, C., Biswas, A., Maemura, T., Trifkovic, S., Babujee, L., Presler, R., Jr., Dahn, R., et al. (2024). Cow's Milk Containing Avian Influenza A(H5N1) Virus - Heat Inactivation and Infectivity in Mice. N Engl J Med *391*, 87-90. 10.1056/NEJMc2405495.

6. Purcell, R., Giles, M.L., Crawford, N.W., and Buttery, J. (2025). Systematic Review of Avian Influenza Virus Infection and Outcomes during Pregnancy. Emerg Infect Dis *31*, 50-56. 10.3201/eid3101.241343.
7. Creisher, P.S., and Klein, S.L. (2024). Pathogenesis of viral infections during pregnancy. Clin Microbiol Rev *37*, e0007323. 10.1128/cmr.00073-23.
8. Xu, L., Bao, L., Deng, W., and Qin, C. (2011). Highly pathogenic avian influenza H5N1 virus could partly be evacuated by pregnant BALB/c mouse during abortion or preterm delivery. Virol J *8*, 342. 10.1186/1743-422X-8-342.
9. Burrough, E.R., Magstadt, D.R., Petersen, B., Timmermans, S.J., Gauger, P.C., Zhang, J., Siepker, C., Mainenti, M., Li, G., Thompson, A.C., et al. (2024). Highly Pathogenic Avian Influenza A(H5N1) Clade 2.3.4.4b Virus Infection in Domestic Dairy Cattle and Cats, United States, 2024. Emerg Infect Dis *30*, 1335-1343. 10.3201/eid3007.240508.
10. CDC (2025). H5 Bird Flu: Current Situation. Avian Influenza (Bird Flu).
11. Uyeki, T.M., Milton, S., Abdul Hamid, C., Reinoso Webb, C., Presley, S.M., Shetty, V., Rollo, S.N., Martinez, D.L., Rai, S., Gonzales, E.R., et al. (2024). Highly Pathogenic Avian Influenza A(H5N1) Virus Infection in a Dairy Farm Worker. N Engl J Med *390*, 2028-2029. 10.1056/NEJMc2405371.
12. CDC (2024). CDC confirms H5N1 Bird Flu Infection in a Child in California. CDC Newsroom.
13. CDC (2024). Technical Update: Summary Analysis of the Genetic Sequence of a Highly Pathogenic Avian Influenza A(H5N1) Virus Identified in a Child in California. Avian influenza (Bird Flu).
14. Petersen, B.A. (2025). High-Pathogenicity (Highly Pathogenic) Avian Influenza in Cattle. Merck Manual.
15. Brooks, R. (2025). Some California Veterinarians Say Virus-Hit Dairies See More Abortions in First-Calf Heifers and Dry Cows. Bovine Veterinarian.
16. Creisher, P.S., Parish, M.A., Lei, J., Liu, J., Perry, J.L., Campbell, A.D., Sherer, M.L., Burd, I., and Klein, S.L. (2024). Suppression of progesterone by influenza A virus mediates adverse maternal and fetal outcomes in mice. mBio *15*, e0306523. 10.1128/mbio.03065-23.
17. McHugh, K.J., Mandalapu, S., Kolls, J.K., Ross, T.M., and Alcorn, J.F. (2013). A novel outbred mouse model of 2009 pandemic influenza and bacterial co-infection severity. PLoS One *8*, e82865. 10.1371/journal.pone.0082865.
18. Vermillion, M.S., Nelson, A., Vom Steeg, L., Loube, J., Mitzner, W., and Klein, S.L. (2018). Pregnancy preserves pulmonary function following influenza virus infection in C57BL/6 mice. Am J Physiol Lung Cell Mol Physiol *315*, L517-L525. 10.1152/ajplung.00066.2018.
19. Sones, J.L., and Davisson, R.L. (2016). Preeclampsia, of mice and women. Physiol Genomics *48*, 565-572. 10.1152/physiolgenomics.00125.2015.
20. Ornoy, A., and Miller, R.K. (2023). Yolk sac development, function and role in rodent pregnancy. Birth Defects Res *115*, 1243-1254. 10.1002/bdr2.2172.
21. Honvo-Houeto, E., and Truchet, S. (2015). Indirect Immunofluorescence on Frozen Sections of Mouse Mammary Gland. J Vis Exp. 10.3791/53179.
22. Liu, S., Sha, J., Yu, Z., Hu, Y., Chan, T.C., Wang, X., Pan, H., Cheng, W., Mao, S., Zhang, R.J., and Chen, E. (2016). Avian influenza virus in pregnancy. Rev Med Virol *26*, 268-284. 10.1002/rmv.1884.
23. Gu, J., Xie, Z., Gao, Z., Liu, J., Korteweg, C., Ye, J., Lau, L.T., Lu, J., Gao, Z., Zhang, B., et al. (2007). H5N1 infection of the respiratory tract and beyond: a molecular pathology study. Lancet *370*, 1137-1145. 10.1016/S0140-6736(07)61515-3.
24. Rusidze, M., Gargaros, A., Febrissy, C., Dubucs, C., Weyl, A., Ousselin, J., Aziza, J., Arnal, J.F., and Lenfant, F. (2023). Estrogen Actions in Placental Vascular Morphogenesis and Spiral Artery Remodeling: A Comparative View between Humans and Mice. Cells *12*. 10.3390/cells12040620.
25. El-Haddad, M.A., Desai, M., Gayle, D., and Ross, M.G. (2004). In utero development of fetal thirst and appetite: potential for programming. J Soc Gynecol Investig *11*, 123-130. 10.1016/j.jsgi.2003.12.001.
26. Le, T.V., Phan, L.T., Ly, K.H.K., Nguyen, L.T., Nguyen, H.T., Ho, N.T.T., Trinh, T.X., and Tran Minh, N.N. (2019). Fatal avian influenza A(H5N1) infection in a 36-week pregnant woman survived by her newborn in Soc Trang Province, Vietnam, 2012. Influenza Other Respir Viruses *13*, 292-297. 10.1111/irv.12614.
27. Carla Fiorito, Ana Colom, Antonio Fernández, Paula Alonso-Almorox, Marisa Andrada, Daniel Lombardo, and Sierra, E. (2025). Pathology of Influenza A (H5N1) infection in pinnipeds reveals novel tissue tropism and vertical transmission. bioRxiv. https://doi.org/10.1101/2025.02.07.636856.
28. Caserta, L.C., Frye, E.A., Butt, S.L., Laverack, M., Nooruzzaman, M., Covaleda, L.M., Thompson, A.C., Koscielny, M.P., Cronk, B., Johnson, A., et al. (2024). Spillover of highly pathogenic avian influenza H5N1 virus to dairy cattle. Nature *634*, 669-676. 10.1038/s41586-024-07849-4.

29. Baker, A.L., Arruda, B., Palmer, M.V., Boggiatto, P., Sarlo Davila, K., Buckley, A., Ciacci Zanella, G., Snyder, C.A., Anderson, T.K., Hutter, C.R., et al. (2025). Dairy cows inoculated with highly pathogenic avian influenza virus H5N1. Nature *637*, 913-920. 10.1038/s41586-024-08166-6.
30. Halwe, N.J., Cool, K., Breithaupt, A., Schon, J., Trujillo, J.D., Nooruzzaman, M., Kwon, T., Ahrens, A.K., Britzke, T., McDowell, C.D., et al. (2025). H5N1 clade 2.3.4.4b dynamics in experimentally infected calves and cows. Nature *637*, 903-912. 10.1038/s41586-024-08063-y.
31. Shi, J., Kong, H., Cui, P., Deng, G., Zeng, X., Jiang, Y., He, X., Zhang, X., Chen, L., Zhuang, Y., et al. (2025). H5N1 virus invades the mammary glands of dairy cattle through "mouth-to-teat" transmission. National Science Review. 10.1093/nsr/nwaf262.
32. Song, J.Y., Park, K.V., Han, S.W., Choi, M.J., Noh, J.Y., Cheong, H.J., Kim, W.J., Oh, M.J., and Cho, G.J. (2020). Paradoxical long-term impact of maternal influenza infection on neonates and infants. BMC Infect Dis *20*, 502. 10.1186/s12879-020-05236-8.
33. Blehar, M.C., Spong, C., Grady, C., Goldkind, S.F., Sahin, L., and Clayton, J.A. (2013). Enrolling pregnant women: issues in clinical research. Womens Health Issues *23*, e39-45. 10.1016/j.whi.2012.10.003.
34. Ramya Naraharisetti, Meghan Weinberg, Becky Stoddard, Mary Grace Stobierski, Kimberly A. Dodd, Nora Wineland, Mathew Beal, Jennifer Morse, Samantha Hatter, Dodd Sledge, et al. (2025). Highly Pathogenic Avian Influenza A(H5N1) Virus Infection of Indoor Domestic Cats Within Dairy Industry Worker Households — Michigan, May 2024. Morbidity and Mortality Weekly Report (MMWR) *74*, 61-65.
35. Fabrizio, T.P., Kandeil, A., Harrington, W.N., Jones, J.C., Jeevan, T., Andreev, K., Seiler, P., Fogo, J., Davis, M.L., Crumpton, J.C., et al. (2025). Genotype B3.13 influenza A(H5N1) viruses isolated from dairy cattle demonstrate high virulence in laboratory models, but retain avian virus-like properties. Nat Commun *16*, 6771. 10.1038/s41467-025-61757-3.
36. Swanson, N.J., Marinho, P., Dziedzic, A., Jedlicka, A., Liu, H., Fenstermacher, K., Rothman, R., and Pekosz, A. (2023). 2019-2020 H1N1 clade A5a.1 viruses have better in vitro fitness compared with the co-circulating A5a.2 clade. Sci Rep *13*, 10223. 10.1038/s41598-023-37122-z.
37. vom Steeg, L.G., Dhakal, S., Woldetsadik, Y.A., Park, H.S., Mulka, K.R., Reilly, E.C., Topham, D.J., and Klein, S.L. (2020). Androgen receptor signaling in the lungs mitigates inflammation and improves the outcome of influenza in mice. PLoS Pathog *16*, e1008506. 10.1371/journal.ppat.1008506.
38. vom Steeg, L.G., Vermillion, M.S., Hall, O.J., Alam, O., McFarland, R., Chen, H., Zirkin, B., and Klein, S.L. (2016). Age and testosterone mediate influenza pathogenesis in male mice. Am J Physiol Lung Cell Mol Physiol *311*, L1234-L1244. 10.1152/ajplung.00352.2016.
39. DePeters, E.J., and Hovey, R.C. (2009). Methods for collecting milk from mice. J Mammary Gland Biol Neoplasia *14*, 397-400. 10.1007/s10911-009-9158-0.
40. Feather-Schussler, D.N., and Ferguson, T.S. (2016). A Battery of Motor Tests in a Neonatal Mouse Model of Cerebral Palsy. J Vis Exp. 10.3791/53569.
41. Reed, L.J., and Muench, H. (1938). A SIMPLE METHOD OF ESTIMATING FIFTY PER CENT ENDPOINTS. American Journal of Epidemiology *27*, 493-497.
42. Zaqout, S., Becker, L.L., and Kaindl, A.M. (2020). Immunofluorescence Staining of Paraffin Sections Step by Step. Front Neuroanat *14*, 582218. 10.3389/fnana.2020.582218.
43. Schindelin, J., Arganda-Carreras, I., Frise, E., Kaynig, V., Longair, M., Pietzsch, T., Preibisch, S., Rueden, C., Saalfeld, S., Schmid, B., et al. (2012). Fiji: an open-source platform for biological-image analysis. Nat Methods *9*, 676-682. 10.1038/nmeth.2019.
44. Parish, M.A., Sachithanandham, J., Gutierrez, L., Park, H.S., Yin, A., Roznik, K., Creisher, P., Lee, J.S., St Clair, L.A., Werner, A., et al. (2025). Pregnancy Reduces COVID-19 Vaccine Immunity Against Novel Variants. medRxiv. 10.1101/2025.01.29.25321357.
45. Bliss, C.M., Freyn, A.W., Caniels, T.G., Leyva-Grado, V.H., Nachbagauer, R., Sun, W., Tan, G.S., Gillespie, V.L., McMahon, M., Krammer, F., et al. (2022). A single-shot adenoviral vaccine provides hemagglutinin stalk-mediated protection against heterosubtypic influenza challenge in mice. Mol Ther *30*, 2024-2047. 10.1016/j.ymthe.2022.01.011.